ELECTRICAL AND OPTICAL CHARACTERIZATION OF AN ARGON-BASED ATMOSPHERIC PRESSURE PLASMA JET UNDER NON-LTE CONDITIONS

Shaleen Kumar Dhital[1]*, **Bhesh Bahadur Thapa**[2], **Raju Bhai Tyata**[2]

[1] Department of Physics, Tri-Chandra Multiple Campus, Kathmandu, Nepal
[2] Department of Sciences and Humanities, Khwopa College of Engineering, Bhaktapur, Nepal

Abstract

This study investigates the generation and detailed characterization of an Argon-based Atmospheric Pressure Plasma Jet (AAPPJ) through systematic electrical and optical diagnostics. Electrical measurements yielded an RMS voltage of 0.79 kV and an RMS current of 5.91 mA, corresponding to a power output of 4.64 W. Analysis of the voltage–current waveforms revealed non-linear discharge behavior indicative of complex plasma dynamics. Optical Emission Spectroscopy (OES) identified emission lines from neutral (Ar I) and singly ionized (Ar II) argon species. Using the Boltzmann plot method, electron excitation temperatures were estimated to be 0.274 eV (Ar I) and 0.302 eV (Ar II). The corresponding electron densities were calculated as 1.043×10^{12} cm^{-3} and 1.001×10^{13} cm^{-3}, respectively. These findings reveal electron densities in the order of 10^{12} cm^{-3}–10^{13} cm^{-3}, consistent with typical atmospheric pressure plasma jets. The close agreement between the excitation temperatures suggests a relatively stable plasma operating under weak non-local thermodynamic equilibrium (non-LTE) conditions. Overall, the study highlights the importance of precise electrical and optical diagnostics in understanding the characteristics of plasma discharge.

Keywords: Argon-based atmospheric pressure plasma jet, Electrical and optical characterization, Non-equilibrium plasma characterization, Electron temperature and density, Spectroscopic analysis of plasma

1. Introduction

1.1. Background

Plasma, often called the fourth state of matter, consists of a collection of charged particles, including ions and electrons, which exhibit collective behavior as a result of their interactions. It is a quasi-neutral gas. After solids, liquids, and gas, plasma constitutes more than 90% of the universe. It comprises many reactive species such as positive ions, negative ions, electrons, free radicals, gas atoms or molecules, photons, ozone, and energetic molecules such as O_2 and N_2. It also includes reactive radicals such as hydroxyl (OH·) and nitric oxide (NO·). It occurs naturally in things such as auroras, lightning, stars, and space and can also be made artificially by heating gases to high temperatures and lowering the pressure to ionize them (Liu et al., 1999). Different types of electrical discharge, such as jets, arc discharges, glow discharges, and dielectric barrier discharges, help produce plasma in the laboratory for certain applications. These discharges ionize molecules and gases, creating free radicals and energized atoms (Klämpfl et al., 2012). Because of their practical benefits in a variety of industries, examples include the surface modification of polymers for biomedical applications (healthcare, plasma biology and medicine) (Darmawati et al., 2019), material processing, nanotechnology (Samukawa, 2022), and pollution control (Kim, 2004), and the simplest configuration and cost-effective generation, AAPPJ, are particularly interesting, often for characterization (Winter et al., 2015).

Numerous AAPJ characterization methods have been invented, and most are based on optical (Zaplotnik et al.,

*Corresponding author: Shaleen Kumar Dhital
Department of Physics, Tri-Chandra Multiple Campus, Kathmandu, Nepal
Email: shaleen.795401@trc.tu.edu.np
(Received: May 18, 2025, Accepted: July 13, 2025)
https://doi.org/10.3126/jsce.v13i2.96561

2015) and electrical characterization (Jovanović et al., 2022). Accurately determining the power consumption, electron density (n_e), and electron temperature (T_e) in plasma is essential to improve analytical performance in various applications, including electrical analysis, spectroscopic analysis, and understanding the basic mechanics behind plasma behavior. Several authors discuss limitations and considerations that must be considered, such as the degree of local thermodynamic equilibrium (LTE), plasma gas purity, and spectral interferences, which can significantly affect the precision of diagnostic techniques (Tabaie et al., 2020). Using theoretical plots and equations, this research seeks to improve the understanding of electron dynamics in Argon (Ar) plasmas and contribute to the development of more precise diagnostic techniques in plasma spectroscopy.

1.2. Theoretical Background

1.2.1 Electrical Characterization of Plasma: Calculation of V_{RMS}, I_{RMS}, and Power (P)

The electrical properties of plasma, including the root mean square (RMS) voltage (V_{RMS}), RMS current (I_{RMS}), and power (P), are fundamental for analyzing plasma behavior and optimizing its applications. These parameters provide insights into energy transfer, discharge stability, and overall plasma efficiency.

i. **Root Mean Square (RMS) Voltage:**
The RMS voltage represents the effective voltage applied across the electrodes and is defined as (Sharma et al., 2024)

$$V_{\text{RMS}} = \sqrt{\frac{1}{T}\int_0^T V^2(t)\,dt} \tag{1}$$

- T is the total time period of observation,
- $V(t)$ is the instantaneous voltage at time t.

ii. **Root Mean Square (RMS) Current:**
The RMS current, describing the actual current flow through the plasma discharge (Sharma et al., 2024), is given by:

$$I_{\text{RMS}} = \sqrt{\frac{1}{T}\int_0^T I^2(t)\,dt} \tag{2}$$

- $I(t)$ denotes the instantaneous current as a function of time.

iii. **Power Calculation in Plasma:**
The power delivered to the plasma is determined as:

$$P = V_{\text{RMS}} \times I_{\text{RMS}} \times \cos(\phi) \tag{3}$$

where, $\cos(\phi)$ accounts for the phase difference between voltage and current in AC-powered plasmas. For resistive plasma conditions, where $\cos(\phi) \approx 1$, the expression simplifies to (Sharma et al., 2024)

$$P = V_{\text{RMS}} \times I_{\text{RMS}} \tag{4}$$

1.2.2 Optical Characterization: Determination of Electron Temperature and Electron Density in Plasma

Determining the electron temperature in a plasma using spectroscopic methods is a well-established challenge, leading to a variety of temperature definitions, each with its own nuances. These include terms such as excitation temperature (T_{exc}), ionization temperature (T_{ion}), LTE temperature (T_{LTE}), and kinetic electron temperature (T_{kin}), among others. However, the same terminology may refer to different methods depending on the context, adding to complexity and confusion (Sijde & Mullen, 1990).

The electron excitation temperature (T_e) is determined using the Boltzmann plot method for Ar I and Ar II species, with data sourced from the NIST database. In this approach, for a plasma in LTE, the equation is given by:

$$ln\left(\frac{\lambda_{ij} I_{ij}}{A_{ij} g_j}\right) = -\frac{E_j}{k_B T_e} + K \tag{5}$$

where, I_{ij} represents the intensity of the transition from state i to j, while λ_{ij} is the corresponding wavelength. The term A_{ij} denotes the transition probability and g_j is the statistical weight. Furthermore, E_j corresponds to the upper energy level, T_e is the electron excitation temperature, and K is a constant. By plotting $\ln\left(\frac{\lambda_{ij} I_{ij}}{A_{ij} g_j}\right)$ against E_j, the slope of the resulting graph, known as the Boltzmann plot, determines the electron excitation temperature (Balcon et al., 2007; Sharma et al., 2024).

Despite these differences, all of these approaches are based on the premise that the kinetic electron temperature influences the density of excited states in the plasma because electron collisions predominantly cause excitation. In an ionization-recombination equilibrium where no particle or energy transport occurs, the exponential factor in the Saha equation can describe the electron temperature (Sijde & Mullen, 1990).

The electron density in the generated discharge is determined using the Boltzmann-Saha equation (Baniya et al., 2020; Shrestha et al., 2016; Tyata et al., 2013):

$$n_e = 2 \times \frac{I_n}{I_+}\frac{\lambda_n A_+ g_+}{\lambda_+ A_n g_n}\left[\frac{2\pi m_e k T_e}{h^2}\right]^{3/2} \exp\left(-\frac{E_a - E_c + E_i}{kT_e}\right) \tag{6}$$

Here, I_n and I_+ denote the intensities of Ar I and Ar II atomic spectral lines, while λ_n and λ_+ are their corresponding wavelengths. The transition probabilities of the the Ar I and Ar II species are represented by A_n and A_+, with their respective statistical weights given by g_n and g_+. Furthermore, E_i corresponds to the ionization energy of the neutral atom. The electron excitation temperature is denoted by T_e, and n_e represents the electron density.

Although the Boltzmann and Saha equations are formally derived under LTE assumptions, they are often applied as diagnostic approximations in non-LTE discharges. In this study, we used these methods with caution, recognizing that the AAPPJ operates under non-LTE conditions, where electron energy distributions may deviate from Maxwellian behavior.

1.3. Objective

This study aims to generate an AAPPJ, characterize its electrical and optical properties, and analyze the discharge process.

1.4. Significance

AAPPJs have demonstrated their potential in materials science and manufacturing, particularly for coating deposition, surface modifications and treatments (Penkov et al., 2015). Additionally, they have gained recognition in biomedical applications as a promising tool for medical treatments.

1.5. Roadmap

In this paper, we present the generation of an AAPPJ, along with its electrical and optical characterization. In addition,we provide a comprehensive analysis of the discharge process.

2. Experimental Details

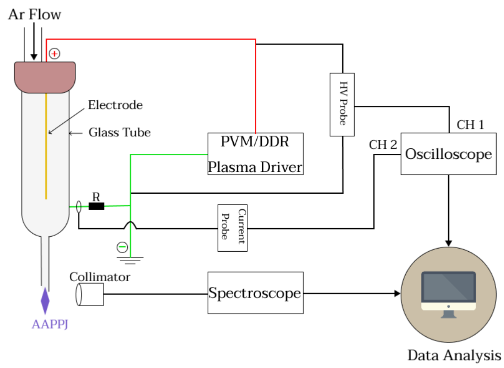

Figure 1. Schematic diagram of the experimental setup.

The schematic diagram of the experimental setup to study AAPPJ is shown in Figure 1. The discharge is generated below the cylindrical electrode inside the glass tube. The electrode is made of borosilicate glass. It has a diameter of 12 mm and height of 100 mm. A PVM/DDR Plasma Driver, consisting of two probes, generates the 2200 V maintaining 29.586 kHz frequency. Argon gas is passed at the rate of 2.5 liter/min through a hollow tube of diameter 7 mm. A high voltage probe is used to measure the voltage applied on the electrode from the channel-1 (**CH 1**), and the discharge current is measured with probe from channel- 2 (**CH 2**) of the plasma driver. The signals are recorded using a Owon SDS7102V digital oscilloscope.

The optical emission spectra in the range 200-1100 nm are recorded by an AvaSpec-ULS3648-USB2-UA-25 spectrometer. Its has 300 grating lines per mm. It has a 3948 pixel CCD detector with 75 mm AVABench. The collimator is placed 1 cm below the orifice of the hollow outlet. Although Ar is 98% pure, the appearance of spectral lines of N_2 and OH should be recognized if present because of the interaction of gaseous plasma with the neighboring atmosphere.

2.1. Electode Design

Figure 2. Photograph of the AAPPJ electrode.

The picture (Figure 2) is a live photograph of discharge of an AAPPJ from the experimental electrode system used in the laboratory. This particular configuration employs a single-electrode setup with argon as the working gas, which is introduced through the designated gas inlet at the top of the system. The use of argon is strategically chosen due to its chemically inert nature, low breakdown voltage, and ability to generate a stable plasma discharge, ensuring minimal interference with target surfaces or substrates, if used in surficial modification.

A cork is positioned between the gas inlet and the discharge tube. This component plays a crucial role in insulating the electrode, preventing unintended electrical discharge while simultaneously allowing the controlled flow of gas. The central element of this set-up is the single copper electrode, which extends into the discharge tube. Copper is selected because of its high electrical conductivity and resistance to oxidation, ensuring efficient energy transfer and sustained plasma generation. Upon applying a high voltage to the electrode, the Argon gas undergoes ionization, forming a plasma plume that exits through the nozzle at the bottom of the discharge tube. The discharge tube, diameter of 12 mm and height of 100 mm, itself is typically composed of dielectric materials, borosilicate glass, which serve to confine and direct the plasma while minimizing heat loss and unwanted charge buildup.

The single-electrode APPJ model offers a simplified but effective approach to plasma generation, making it a valuable configuration for various applications (Zaplotnik et al., 2015). Its design facilitates ease of operation and adaptability while maintaining sufficient control over plasma parameters.

3. Result and Discussion

3.1. Electrical Characterization of Atmospheric Pressure Plasma Jet

The electrical characterization of the plasma gives information about the current and voltage waveform of the discharge produced. The electrical characterization of the AAPPJ is subdivided into parts as follows:

3.1.1 Voltage and Current Waveform

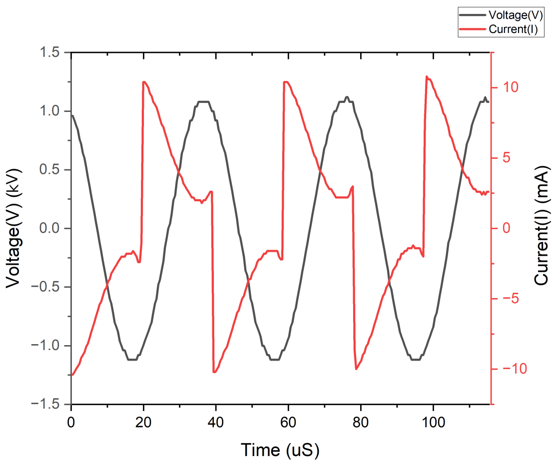

Figure 3. Voltage and current waveform of AAPPJ produced with power supply operated at 29.586KHz.

Figure 3 presents the voltage and current waveforms corresponding to the discharge generated by an AAPPJ. The photograph of the AAPPJ discharge is shown in Figure 4. The current waveform exhibits a displacement current with a maximum amplitude of approximately 10.4 mA, occurring before the peak voltage. The applied voltage increases progressively, reaching a maximum of 1.08 kV.

The current waveform is characterized by two distinct spikes per half cycle: the primary spike reaches a peak displacement of 10.4 mA, while the secondary spike attains a magnitude of 3 mA. It is observed that as the current amplitude decreases from 10.4 mA to 3 mA, the voltage waveform reaches its peak value of 1.08 kV.

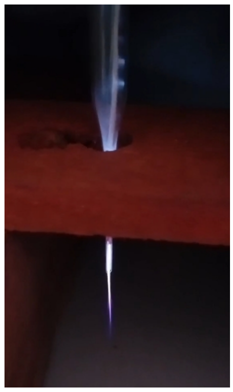
Figure 4. AAPPJ discharge.

Following this, the negative half-cycle of the current waveform reaches its minimum shortly after the voltage peaks, maintaining the alternating cycle over time. The calculated values of RMS current, RMS voltage, and power from (1), (2), and (4) are 0.79 kV, 5.91 mA, and 4.64 watts, respectively.

3.1.2 Power Consumption

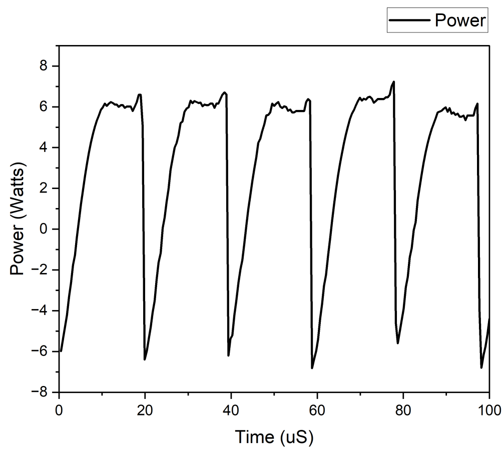

Figure 5. Graphical representation of power consumption of APPJ produced.

The graph (Figure 5) illustrates the temporal variation of the power in a periodic discharge system. The x-axis represents time in microseconds (µs), while the y-axis denotes power in watts (W). The power waveform exhibits a cyclic behavior, oscillating between positive and negative values, indicating an alternating or pulsed power system, likely associated with plasma generation.

The waveform begins at a negative power value of approximately -5.984 W and rises steeply into the positive region. Upon reaching the plateau phase, the power fluctuates within the range of 6.160 to 6.592 W, indicating slight variations at the peak. After maintaining this plateau momentarily, the power sharply drops, reaching a minimum of approximately -6.400 W before rising again into the next cycle. In the subsequent positive plateau, the power oscillates between 6.304 W and 6.704 W before another steep decline into the negative cycle. This pattern of periodic oscillations continues, forming a repeated power cycle.

The presence of these plateaus with slight fluctuations suggests transient effects or minor instabilities in the power delivery, possibly due to variations in plasma discharge conditions. The symmetric nature of the waveform indicates that the system operates under a controlled alternating power mechanism, where energy is periodically supplied and dissipated. Such power behavior is characteristic of AAPPJ or similar high-frequency discharge systems, where rapid power modulation is necessary to maintain a stable plasma state.

3.1.3 I-V nature

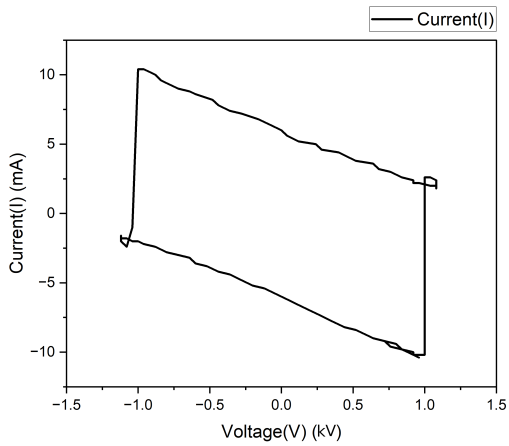

Figure 6. I-V plot.

The voltage-current (V-I) characteristic curve (Figure 6) of the AAPPJ provides critical insights into its electrical behavior, including power dissipation and charge dynamics. The plot exhibits a closed-loop trajectory, indicative of the capacitive and resistive nature of the discharge under alternating current (AC) conditions. Sharp transitions at the extremities highlight the nonlinear plasma behavior, where charge accumulation and conduction mechanisms govern the discharge dynamics.

The V-I plot forms a parallelogram-like structure, with primary edges defined by the points (-1, 10.4) and (1, -10.2), marking the voltage and current boundaries. Unlike conventional Lissajous figures, this plot lacks loops along its edges, suggesting abrupt current transitions as the voltage approaches its maximum and minimum values. Within the main structure, two distinct internal loops are observed, attributed to charge redistribution and energy dissipation processes. The first loop, located in the negative voltage region, is characterized by the points (-1.08, -1.80), (-1.08, -2.4), and (-1.12, -1.80), with a sharp spike at the final point, indicative of transient effects. The second loop, appearing in the positive voltage region, comprises (1.08, 2.4), (1, 2.6), and (1.08, 2), with a similar sharp spike observed at the last point.

These internal loops reveal localized instabilities and rapid changes in plasma conductivity, reinforcing the presence of transient charge dynamics. Such features point to complex ionization processes and rapid carrier motion within the discharge channel. The absence of smooth transitions along the edges further supports the view of abrupt shifts between charging and discharging phases. Overall, the curve illustrates the intricate interplay between the applied electric field and the plasma response under atmospheric conditions. The area enclosed within the parallelogram corresponds to the power dissipated in the plasma, making this analysis significant for optimizing discharge characteristics and enhancing the performance of plasma-based applications.

3.2. Optical Characterization of Atmospheric Pressure Plasma Jet

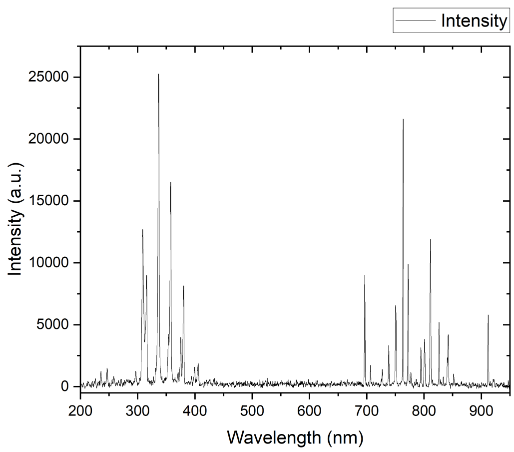

Figure 7. Optical emission spectrum of atmospheric pressure plasma jet for wavelength ranging from 200-1100 nm.

Optical Emission Spectroscopy (OES) is a widely used technique for measuring light intensity across various wavelengths, providing insights into the excited states of atoms and molecules. This data is crucial for determining key plasma properties such as electron excitation temperature and density. The intensity variations across wavelengths are shown in Figure 7, categorized into two ranges: (a) is for the wavelength ranging from 200 nm to 450 nm, and (b) is for the range of 690 nm to 915 nm as shown in Figure 8.

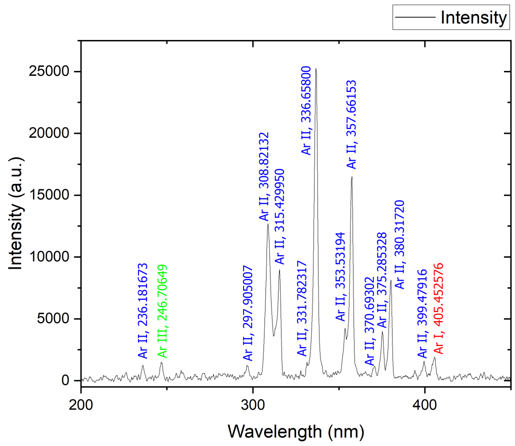

(a)

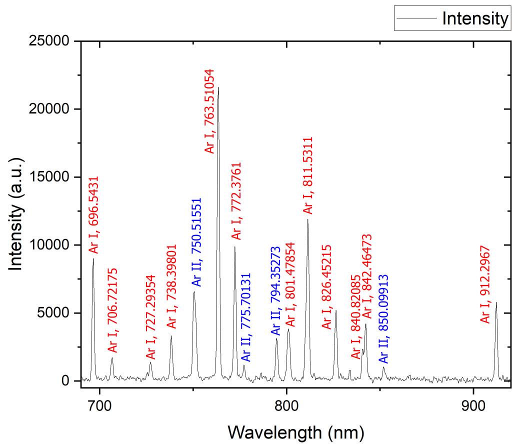

(b)

Figure 8. Optical emission spectrum of atmospheric pressure plasma jet in different wavelength ranges.

The different spectral lines of Argon [Ar I, in red, and Ar II, in blue, as in Figure 8 are used to calculate the electron excitation temperature, and the electron density. Table 1 and Table 2 show the spectral lines with corresponding wavelength, statistical weight, energy level, and transition probability.

Using the the Boltzmann equation (5) these data, the electron excitation temperature is determined by applying the Boltzmann plot method, where $\ln\left(\frac{\lambda_{ij} I_{ij}}{A_{ij} g_j}\right)$ is plotted against the upper energy level E_j. The slope of the linear fit to this plot provides the excitation temperature of the electrons. A sample Boltzmann plot used to derive the electron temperature is illustrated in Fig. 9 and Fig. 10. Once the electron temperature is obtained, the electron density can be calculated using (6).

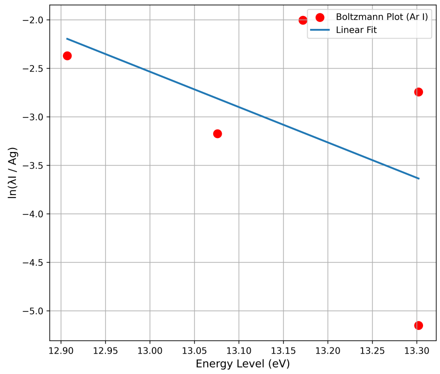

Figure 9. Boltzmann Plot for Ar I.

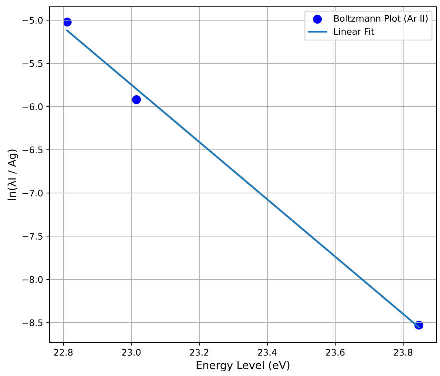

Figure 10. Boltzmann plot for Ar II.

The electron excitation temperature of the Argon plasma was determined, which relates the logarithm of the normalized line intensity to the corresponding upper energy level of the transition. Linear fits were applied using four samples of emission line from tables to spectral data for both neutral argon (Figure 9), and singly ionized argon (Figure 10). The slope obtained for Ar I was -3.645, and for Ar II, it was -3.317, where the slope corresponds to the inverse of the product of the Boltzmann constant and electron temperature.

Based on these slopes, the electron excitation temperatures were calculated to be approximately 3183.995 K or 0.274 eV for Ar I and 3498.342 K or 0.302 eV for Ar II.

Using (6), the electron density (n_e) can then be calculated by substituting the value of electron temperature. Here, I_n is

Table 1. Observed Ar I peaks in optical emission spectroscopy of AAPPJ and its corresponding spectroscopic data from NIST database for plotting of Boltzmann plot.

λ_{ij} **(nm)**	A_{ij} **(s^{-1})**	E_j **(eV)**	$g_i - g_j$
405.452	2.70×10^4	14.681	3–3
696.543	6.40×10^6	13.328	5–3
706.722	3.80×10^6	13.302	5–5
727.294	1.83×10^6	13.328	3–3
738.398	8.50×10^7	13.302	3–5
763.511	2.45×10^7	13.172	5–5
772.376	5.20×10^7	13.153	5–3
811.531	3.30×10^7	13.076	5–7
826.452	1.53×10^7	13.328	3–3
840.821	2.23×10^7	13.302	3–5
842.465	2.15×10^7	13.095	3–5
912.297	1.89×10^7	12.907	5–3

Table 2. Observed Ar II peaks in optical emission spectroscopy of AAPPJ and its corresponding spectroscopic data from NIST database for plotting of Boltzmann plot.

λ_{ij} **(nm)**	A_{ij} **(s^{-1})**	E_j **(eV)**	$g_i - g_j$
336.658	4.10×10^7	23.549	4–2
353.532	5.70×10^7	22.811	2–4
357.662	2.75×10^8	23.015	6–8
370.693	2.00×10^5	19.801	2–2
380.317	1.50×10^8	24.757	6–6
399.479	1.60×10^8	23.846	2–2

the intensity of the Ar I line (706.722 nm) (transition $a \to b$), I_+ is the intensity of the Ar II line (353.532 nm) (transition $c \to d$), and λ_n, λ_+, A_n, and A_+ are the wavelengths and probabilities of the transition. The calculated value of electron density obtained is

$$n_e = 1.043 \times 10^{12}\ \text{cm}^{-3} \text{ for } T_e = 0.274 \text{ eV}$$

and

$$n_e = 1.001 \times 10^{13}\ \text{cm}^{-3} \text{ for } T_e = 0.302 \text{ eV}.$$

The electron densities calculated independently from neutral argon (Ar I) and singly ionized argon (Ar II) emission lines were found to be of the order of 10^{12} cm^{-3} and 10^{13} cm^{-3}, respectively. The close agreement between the corresponding excitation temperatures suggests near-equilibrium excitation behavior, while the slight variation in the estimated electron densities indicates weak nonlocal thermodynamic equilibrium (non-LTE) characteristics within the plasma discharge.

Such weak non-LTE behavior is commonly observed in Atmospheric Pressure Plasma Jets (APPJs), where frequent collisional interactions and spatial or temporal energy gradients influence plasma kinetics. The obtained electron densities, in the order of 10^{12}–10^{13} cm^{-3}, are consistent with values typically reported for low-power atmospheric pressure argon plasma jets, supporting the reliability of the present diagnostic approach and the measured plasma parameters.

4. Conclusion

This study investigated the generation and characterization of an AAPPJ through detailed electrical and optical diagnostics. The results underscore the importance of precise measurement techniques for understanding plasma behavior, crucial for optimizing applications in materials science and biomedical treatments.

Electrical characterization revealed discharge dynamics, with an RMS voltage and RMS current, corresponding to a power output. The non-linear voltage-current (V-I) characteristics reflected the complex interactions within the plasma, which are significant for applications requiring fine plasma control.

The optical diagnostics confirmed the generation of a stable and weakly ionized plasma, with the extracted plasma parameters indicating electron densities within the typical range for low-power atmospheric pressure plasma jets. The close agreement between the excitation characteristics obtained from neutral and singly ionized argon transitions suggests near-equilibrium excitation behavior, while the observed variation in electron density reflects the inherent weak nonlocal thermodynamic equilibrium (non-LTE) nature of atmospheric pressure discharges. These findings demonstrate the reliability of the applied spectroscopic approach in characterizing the plasma state and provide valuable insight into the discharge kinetics of the developed AAPPJ system.

These findings confirm the effectiveness of combined electrical and spectroscopic diagnostics in understanding plasma behavior and accurately characterizing discharge properties. The obtained plasma parameters further demonstrate the potential of AAPPJs for applications in surface modification, material processing, and biomedical treatments. Future work will focus on optimizing plasma jet configurations, investigating alternative working gas mixtures, and employing time-resolved diagnostics to gain deeper insight into transient plasma phenomena.

Acknowledgments

We gratefully acknowledge Khwopa College of Engineering for granting access to their plasma laboratory and essential equipments. The unwavering support and guidance from the faculty and staff played a vital role in the successful execution of this research.

References

Balcon, N., Aanesland, A., & Boswell, R. (2007). Pulsed rf discharges, glow and filamentary mode at atmospheric pressure in argon. *Plasma Sources Science and Technology*, *16*(2), 217.

Baniya, H., Guragain, R., Panta, G., Safaai, S., Dhungana, S., Qin, G., & Subedi, D. (2020). Investigation on parameters of atmospheric pressure plasma jet by electrical and optical methods. *Journal of Nepal Physical Society*, *6*(2), 50–56.

Darmawati, S., Rohmani, A., Nurani, L. H., Prastiyanto, M. E., Dewi, S. S., Salsabila, N., Wahyuningtyas, E. S., Murdiya, F., Sikumbang, I. M., Rohmah, R. N., Fatimah, Y. A., Widiyanto, A., Ishijima, T., Sugama, J., Nakatani, T., & Nasruddin, N. (2019). When plasma jet is effective for chronic wound bacteria inactivation, is it also effective for wound healing? *Clinical Plasma Medicine*, *14*, 100085. https://doi.org/https://doi.org/10.1016/j.cpme.2019.100085

Jovanović, O., Nevena, P., & Škoro, N. (2022). A comparison of power measurement techniques and electrical characterization of an atmospheric pressure plasma jet. *Plasma Science and Technology*, *24*(10), 105404. https://doi.org/10.1088/2058-6272/ac742b

Kim, H.-H. (2004). Nonthermal plasma processing for air-pollution control: A historical review, current issues, and future prospects. *Plasma Processes and Polymers*, *1*(2), 91–110. https://doi.org/https://doi.org/10.1002/ppap.200400028

Klämpfl, T. G., Isbary, G., Shimizu, T., Li, Y.-F., Zimmermann, J. L., Stolz, W., Schlegel, J., Morfill, G. E., & Schmidt, H.-U. (2012). Cold atmospheric air plasma sterilization against spores and other microorganisms of clinical interest. *Applied and Environmental Microbiology*, *78*(15), 5077–5082. https://doi.org/10.1128/AEM.00583-12

Liu, C.-j., Xu, G.-h., & Wang, T. (1999). Non-thermal plasma approaches in co2 utilization. *Fuel Processing Technology*, *58*(2), 119–134. https://doi.org/https://doi.org/10.1016/S0378-3820(98)00091-5

Penkov, O. V., Khadem, M., Lim, W.-S., & Kim, D.-E. (2015). A review of recent applications of atmospheric pressure plasma jets for materials processing. *Journal of Coatings Technology and Research*, *12*(2), 225–235. https://doi.org/10.1007/s11998-014-9638-z

Samukawa, S. (2022). Emerging plasma nanotechnology. *IEEE Open Journal of Nanotechnology*, *3*, 133–148. https://doi.org/10.1109/OJNANO.2022.3217806

Sharma, S., Chalise, R., Basnet, S., Lamichhane, H. P., & Khanal, R. (2024). Development of a low-cost plasma source using fly-back transformer for atmospheric pressure gliding arc discharge. *Physics of Plasmas*, *31*(4), 043509. https://doi.org/10.1063/5.0187159

Shrestha, R., Subedi, D., Gurung, J., & Wong, C. (2016). Generation, characterization and application of atmospheric pressure plasma jet. *Sains Malaysiana*, *45*(11), 1689–1696.

Sijde, B., & Mullen, J. (1990). Temperature determination in non-lte plasmas [Special Issue Spectral Line Formation in Plasmas Under Extreme or Unusual Conditions]. *Journal of Quantitative Spectroscopy and Radiative Transfer*, *44*(1), 39–46. https://doi.org/https://doi.org/10.1016/0022-4073(90)90079-L

Tabaie, S., Iraji, D., & Amrollahi, R. (2020). Measurement of electron temperature and density of atmospheric plasma needle. *Vacuum*, *182*, 109761. https://doi.org/https://doi.org/10.1016/j.vacuum.2020.109761

Tyata, R. B., Subedi, D. P., Shrestha, R., & Wong, C. S. (2013). Generation of uniform atmospheric pressure argon glow plasma by dielectric barrier discharge. *Pramana*, *80*(3), 507–517. https://doi.org/10.1007/s12043-012-0494-z

Winter, J., Brandenburg, R., & Weltmann, K.-D. (2015). Atmospheric pressure plasma jets: An overview of devices and new directions. *Plasma sources science and technology*, *24*(6), 064001.

Zaplotnik, R., Biščan, M., Krstulović, N., Popović, D., & Milošević, S. (2015). Cavity ring-down spectroscopy for atmospheric pressure plasma jet analysis. *Plasma Sources Science and Technology*, *24*(5), 054004. https://doi.org/10.1088/0963-0252/24/5/054004